Bio-optical characteristics of the snow, ice, and water column of a perennially ice-covered lake in the High Arctic

Claude Belzile, Warwick F. Vincent, John A.E. Gibson, and Patrick Van Hove

Abstract: Lake A is a meromictic, perennially ice-covered lake located at the northern limit of North America (latitude 83°N, Ellesmere Island, Canada). In early June 1999, only 0.45% of incident photosynthetically available radiation (PAR) was transmitted through its 2-m ice and 0.5-m snow cover. Removal of snow from 12 m^2 increased PAR under the ice by a factor of 13 and biologically effective ultraviolet radiation (UVR) by a factor of 16 (from 0.4% to 6.3% of incident). The diffuse attenuation coefficient (K_d) for UVR was substantially lower in the ice than in the underlying freshwater (e.g., 50% lower at 320 nm), indicating the exclusion of chromophoric dissolved organic matter (CDOM) during freeze-up or the subsequent degradation of CDOM retained in the ice. Peak phytoplankton concentrations occurred immediately under the ice, and a broad maximum of photosynthetic sulfur bacteria and associated sulfur particles was observed over the depth interval 20–45 m at <0.005% of incident PAR. Climate-induced changes in the overlying snow and ice have the potential to cause major habitat disruption (UV exposure, PAR, temperature, mixing regime) for these stratified, extreme-shade communities.

Résumé : Le lac A est un lac méromictique couvert de glace en permanence et situé à la limite boréale du continent nord-américain (latitude 83°N, île d'Ellesmere, Canada). Au début de juin 1999, seulement 0,45 % de la radiation incidente disponible pour la photosynthèse (PAR) pénétrait la couche de 2 m de glace recouverte de 0,5 m de neige. Le retrait de la neige sur une surface de 12 m^2 a augmenté la PAR d'un facteur de 13 et la radiation ultraviolette (UVR) à effets biologiques, d'un facteur de 16 (de 0,4 % à 6,3 % de la radiation incidente). Le coefficient d'atténuation (K_d) de l'UVR était considérablement moins élevé dans la glace que dans l'eau douce sous-jacente (e.g. 50 % plus faible à 320 nm), ce qui indique une exclusion de la matière organique dissoute colorée (CDOM) lors du gel ou la dégradation subséquente de la CDOM retenue dans la glace. Les concentrations maximales de phytoplancton se trouvaient juste sous la glace et la densité maximale des bactéries sulfureuses photosynthétiques et des particules de soufre associées s'étalait dans l'intervalle des profondeurs de 20–45 m, à moins de 0,005 % de la PAR incidente. Les changements dans la couverture de neige et de glace générés par le climat peuvent potentiellement causer des modifications majeures de l'habitat (exposition à l'UV, PAR, température, régime de brassage) dans ces communautés stratifiées acclimatées à de faibles intensités lumineuses.

[Traduit par la Rédaction]

Introduction

Perennially ice-covered lakes are an important limnological feature of Antarctica and have proved to be useful model systems for exploring general concepts in geophysics, geochemistry, and microbial ecology. In recognition of this value, a series of such lakes in the McMurdo Dry Valleys region is now the site of a long-term ecological research program (LTER; Priscu 1998). It is less widely known, however, that lakes covered by multiyear ice are also found in the north polar region. Several lakes on northern Ellesmere Island are thought to be perennially ice covered (Ludlam 1996) and other lakes in the High Arctic retain their ice cover throughout summer in some years (e.g., Doran et al. 1996). Our aim in the present study was to evaluate the ice cover and water-column properties of one such north polar lake, Lake A in the Canadian High Arctic, with emphasis on its bio-optical properties relative to analogous lakes in the south polar region.

Ice and snow cover high latitude lakes for more than 8 months of the year and have a broad range of effects on the physical and biological properties of these ecosystems. The presence of ice isolates the water from wind-induced mixing, and thick snow and ice may also inhibit convective processes. This reduced mixing in turn affects the vertical distribution of gases, nutrients, and planktonic organisms (Wharton et al. 1993; Priscu et al. 1999*a*). The effects of ice and snow cover on radiative transfer also regulate biological productivity by controlling photosynthetically available radiation (PAR), exposure to ultraviolet radiation (UVR), and water temperature. Despite this pervasive influence on limnological processes in northern lakes, little attention has been given to the bio-optics of freshwater ice and snow.

The High Arctic is currently subject to major changes in

Received May 8, 2001. Accepted October 24, 2001. Published on the NRC Research Press Web site at http://cjfas.nrc.ca on December 14, 2001.
J16340

C. Belzile,[1] W.F. Vincent, J.A.E. Gibson, and P. Van Hove. Département de biologie and Centre d'études nordiques, Université Laval, Sainte-Foy, QC G1K 7P4, Canada.

[1]Corresponding author (e-mail: claude.belzile@bio.ulaval.ca).

 DOI: 10.1139/cjfas-58-12-2405

climate. The most striking evidence of change has been in records of the extent and thickness of multiyear sea ice across the Arctic Ocean. Over the period 1978 to 1998, the multiyear sea-ice cover diminished in area by 14% in winter (Johannessen et al. 1999) and by 44% in average thickness during the past three decades (Rothrock et al. 1999). An extensive ice shelf (>10-m-thick sea ice) along the northern coast of Ellesmere Island retreated by 90% over the course of the 20th century, with evidence of substantial thinning of the remaining landfast ice in the 1980s and 1990s (Vincent et al. 2001). Continental High Arctic meteorological records also show evidence of change. Temperature data from Arctic stations over the period 1966–1995 indicate a general warming trend, with the greatest effects in the western Arctic (up to 0.7°C per decade; Weller 1998). There is wide regional variability in precipitation trends, from significant increases at certain locations (e.g., Spitsbergen; Hanssenbauer and Forland 1998) to significant decreases at other sites (e.g., Alaska; Curtis et al. 1998). This climatic change is likely to have an impact on lake ecosystems via shifts in snow and ice cover (e.g., Doran et al. 1996) and highlights the need for improved understanding of the properties of these lake ecosystem components.

The High Arctic is also experiencing changes in its incident UV radiation flux. During spring, the increases in surface erythemal UVR resulting from severe chemical ozone losses observed in the Arctic during winter are estimated to be about 22% relative to the values in the 1970s (Madronich et al. 1998). This increase is likely to worsen in duration and severity in the future, in part associated with greenhouse gas effects on stratospheric cooling (Shindell et al. 1998).

Although many modeling and field studies have addressed the variations of snow and ice albedo, little is known about the transmission of UVR through snow and freshwater ice, and even the PAR attenuation characteristics of these media are poorly understood. Clean, fresh, cold snow has a high albedo (>0.9) and is therefore relatively opaque to PAR (Perovich et al. 1998); however, during the aging of the snow or when it becomes wet or covered by wind-blown particles, the PAR albedo can drop substantially (Grenfell and Maykut 1977; Perovich et al. 1998). The UVR albedo of snow is lower than that for PAR (Perovich et al. 1998). The measured diffuse attenuation coefficients for PAR, K_d(PAR), of snow are highly variable depending on snow density, grain size, temperature, and wetness (Thomas 1963; Grenfell and Maykut 1977). To our knowledge, no K_d(UVR) values for snow have been published to date. K_d(PAR) of thick perennial ice has been reported to be as low as 0.2 m^{-1} for Antarctic lakes (Howard-Williams et al. 1998), and transmission of incident PAR through snow-free, 1.5- to 2.2-m-thick clear ice was shown to be as high as 21–35% for High Arctic lakes (Welch and Kalff 1974; Bolsenga et al. 1996). The limited available literature (Ellis-Evans et al. 1998; fig. 4 in Howard-Williams et al. 1998) suggests that UVR transmission through clear ice can be of the same order of magnitude, or greater, than PAR transmission. This may result from the strong within-ice attenuation of the red part of the PAR spectrum. Kepner et al. (2000), however, found low UV transmission through the ice cover of Lake Hoare in the McMurdo Dry Valleys (<0.6% at 320 nm), and this was attributed to the extremely degraded, highly scattering ice surface and the high concentrations of sediment on and within this 4- to 5-m-thick ice. Significant under-ice UVR has been measured in other Antarctic Dry Valleys lakes despite >3-m-thick ice (Vincent et al. 1998); however, there have been no equivalent measurements in Arctic freshwater ecosystems.

In the present study, we addressed the hypothesis that High Arctic lakes may be sensitive to environmental change by virtue of their overlying snow and ice. We undertook measurements of UVR and PAR transmission through the snow and ice cover and of optical properties of the underlying water column of perennially ice-covered Lake A on northern Ellesmere Island. We selected Lake A because it lies at the northern limit of Arctic lakes where future climate changes and ozone depletion are likely to be pronounced.

Materials and methods

Study site

Lake A is located on northern Ellesmere Island (83°00′N, 75°27′W; Fig. 1) in a polar desert region with mean annual precipitation of 157 mm and mean annual temperature of –17.9°C (Table 1). This precipitation is much greater than that in the McMurdo LTER (≤50 mm) at a comparable latitude in Antarctica (78°S), but the mean annual temperature is similar to that in the McMurdo lakes region (–17°C to –19°C; Doran et al. 1994). Table 1 summarizes the mean values for climate variables for the period 1951–1999 at Alert, the nearest available meteorological station, 180 km from Lake A (no local data are available as yet from the lake basin). Lake A was first sampled in 1969 by Geoffrey Hattersley-Smith's group (Hattersley-Smith et al. 1970) and was the object of work in 1982 (Jeffries et al. 1984) and 1993 (Ludlam 1996). The lake depth is >115 m (deepest measured point) and has an area of 4.9 km^2 and a glacier-free drainage basin with an area of 36 km^2. A short outlet stream flows from the northernmost point of the lake to an epishelf lake dammed by the Ward Hunt Ice Shelf. The lake is 3.3 m above sea level and was cut off from the sea following isostatic uplift approximately 3000 years ago, thereby producing the current meromictic conditions (Hattersley-Smith et al. 1970; Jeffries et al. 1984). The conductivity of the monimolimnion is approximately the same as seawater and its ionic composition is that of modern ocean water although modified by biological activity; it is depleted in sulfate and enriched in dissolved inorganic carbon by microbial activity (Jeffries et al. 1984). The monimolimnion and mixolimnion are separated by a chemocline that extends from 7 to 25 m. A thermal maximum of 8–9°C occurs at ~15 m and the waters are anoxic below 14 m (Ludlam 1996). Lake A is covered by 2-m-thick ice, with a candled ice surface resulting from the summertime partial melting (Hattersley-Smith et al. 1970). A narrow moat opens around the ice pan during summer, at least in some years. On August 5, 2001, the moat was 1–10 m wide, except on the eastern side of the lake at the site of the main inflowing stream where the moat was about 100 m wide (C. Belzile and P. Van Hove, personal observation). RADARSAT data for one of the warmest summers on record (1998; Vincent et al. 2001) show the persistence of Lake A ice in late August, whereas the nearby Taconite Inlet lakes (40 km southwest of Lake A) lost their ice cover (Fig. 2). However, the moat on the northern shore of Lake A was much wider (30–120 m; Fig. 2) than observed in 2001. Lake A was covered by ice during late summer, or candled ice was present under the snow in early summer (indicating multiyear ice cover), on each of 11 years of observations during the period 1950–2001.

Sampling

Lake A was sampled during the period of 3–8 June 1999. This time of the year is characterized by continuous daylight and the solar

Fig. 1. Map showing the location of Lake A, northern Ellesmere Island, Canada.

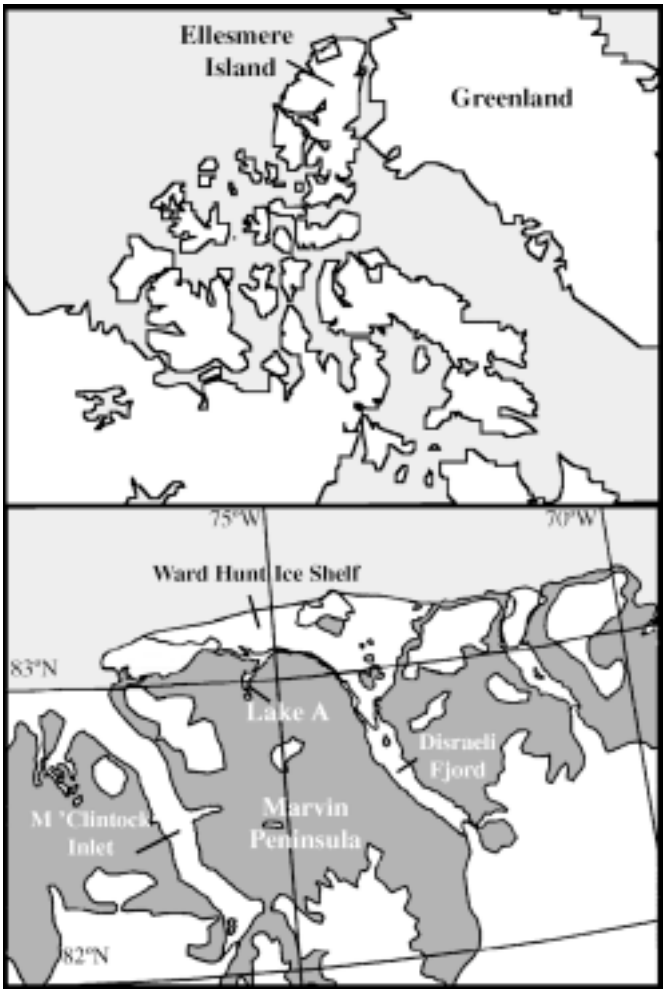

elevation varies from 13 to 33° over the 24-h cycle. Air temperatures at Alert varied from –0.5°C to –10.5°C during the 6 days. Water samples were obtained from 25 selected depths over the deepest part of the lake using a Kemmerer sampling bottle (length = 31 cm) and were stored in dark Nalgene bottles until filtration 1–3 h later at our base camp. Profiles of temperature, specific conductivity, and dissolved oxygen were made using a Hydrolab Surveyor 3 (Hydrolab Corp., Austin, Tex.). Data were recorded at discrete depths to allow stabilization of the instrument; measurements were made every metre from 2 to 13 m and every 50 cm down to 47.5 m (the full length of the profiler cable). Specific conductivity readings were converted to salinity using the algorithm of Fofonoff and Millard (1983). This algorithm is the equation of state for seawater and is applicable over the salinity range of 2–40. Terrestrial input, differential diffusion, and biological processes will alter the ionic composition of the water, but with the exception of the surface waters, this variation should be minor considering that the water in the lake is largely marine derived (Jeffries et al. 1984). The thickness of the ice was measured in five holes distributed over the central region of the lake (spaced by at most 500 m). Snow depth was measured at the site of transmittance measurements (n = 15 over a 12-m^2 area) and every 1 m along a 20-m transect nearby this site. All optical measurements (described below) were made within 5 h of local noon (solar elevation between 25 and 33°) during clear sky conditions or high light clouds.

Albedo measurements

The snow and cleared-ice albedo ($\alpha(\lambda)$), i.e., the ratios of upwelling irradiance (E_u) to downwelling irradiance (E_d), were measured using a PUV510 radiometer (Biospherical Instruments, Inc., San Diego, Calif.) at the same site as the transmittance measurements (see below). The PUV510 measured cosine-corrected UVR at 305, 320, 340, and 380 nm (full bandwidth at half maximum of 8–10 nm) and PAR (400–700 nm). The radiometer was mounted on a 3-m-long pole, which allowed the measurement of E_d and E_u at a height of 1 m over the snow or ice surface.

Irradiance transmittance through the ice and snow cover

The transmittance of the snow and ice ($T(\lambda)$) was calculated as the ratio of downwelling irradiance of wavelength λ at the lower surface of the ice ($E_d(z_{ice}, \lambda)$) to the incident irradiance ($E_d(0^+, \lambda)$). Transmittance depends on the specular and volume components of the albedo and on the attenuation of irradiance by snow and ice according to Beer's Law. For these transmittance measurements, the PUV510 was installed in an unshaded location on the lake ice, and an underwater radiometer (PUV500, Biospherical Instruments, Inc.) was positioned to measure simultaneously the cosine-corrected, under-ice irradiance. The PUV500 recorded irradiance at the same wavelengths as the PUV510 and also recorded depth and temperature. Underwater irradiance measurements were corrected for dark current by subtracting the value obtained at in situ temperatures within the water column after fitting the radiometer with a light-tight Neoprene cap. The PUV500 radiometer was positioned under the ice through a 65-cm-diameter hole using an articulated arm designed in our laboratory. The aluminum arm allowed the positioning of the radiometer flush with the lower ice surface at a distance of 1 m from the hole. During the measurements, the hole was tightly covered with an opaque plastic board, 1 m^2 in area, to prevent direct solar radiation from entering the ice sheet through the hole. Great care was taken to preserve the integrity of the snow cover over the area where the measurements were made in order to obtain transmittance through the natural ice and snow cover. The snow cover was then removed from an area of 12 m^2, and the measurements were repeated under that area to estimate transmittance of only the ice.

Snow and ice attenuation coefficients

The attenuation of irradiance in ice calculated from radiative transfer models is often characterized by the asymptotic extinction coefficient $K_{asym}(\lambda)$ (e.g., Grenfell 1991). In an optically thick medium, the asymptotic state, where the shape of the light field is axially symmetric and does not change, should be approached far from the upper boundary. $K_{asym}(\lambda)$ is difficult to measure in the field and small-scale variability in the physical, biological, and thus optical properties of the ice makes it difficult for the light distribution to remain in the asymptotic state (see Perovich et al. 1998). One simpler way of characterizing irradiance attenuation in ice from field measurements is the "effective" extinction coefficient (Grenfell 1991). This effective downwelling diffuse attenuation coefficient ($K_d(\lambda)$, m^{-1}) for ice can be calculated as

$$(1) \qquad K_d(\lambda)_{ice} = -\ln(E_d(\lambda, z_{ice})/E_d(\lambda, 0^-))/z_{ice}$$

where $E_d(\lambda, z_{ice})$ is the under-ice downwelling irradiance measured in the absence of snow and $E_d(\lambda, 0^-)$ is the downwelling irradiance just below the surface given by

$$(2) \qquad E_d(\lambda, 0^-) = E_d(\lambda, 0^+)\ (1 - \alpha(\lambda)_{ice})$$

where $\alpha(\lambda)_{ice}$ is the albedo of the ice surface (Grenfell 1991). Knowing $K_d(\lambda)_{ice}$, snow $K_d(\lambda)$ can similarly be calculated as

$$(3) \qquad K_d(\lambda)_{snow} = -\ln(E_d(\lambda, z_{snow})/E_d(\lambda, 0^-))/z_{snow}$$

where $E_d(\lambda, z_{snow})$ is the spectral downwelling irradiance at the snow–ice interface given by

Table 1. Mean, minimum, and maximum for meteorological data from Alert over the period 1951–1999.

	Mean	Minimum	Maximum
Precipitation (mm)	157	93	291
Temperature (°C)	–17.9	–19.5	–15.8
Onset of melt (date)	17 June	4 June	1 July
Onset of freeze (date)	21 August	7 August	5 September
Length of melt season (days)	65	43	85
Freezing degree-days	6736	5988	7247
Thawing degree-days	200	104	336

Note: Following Rigor et al. (2000), the length of the melt season was computed from the daily average temperature by using a 2-week running mean filter and defining the onset of melt and freeze as the day that the filtered data rose or dropped below the melting temperature of snow and freshwater ice (0°C).

Fig. 2. RADARSAT-1 images of northern Ellesmere Island acquired on 30 August 1998. On the right, ice-covered Lake A and Lake B are shown. For comparison, on the left, ice-free lakes of the Taconite Inlet region, 40 km to the southwest of Lake A, are shown.

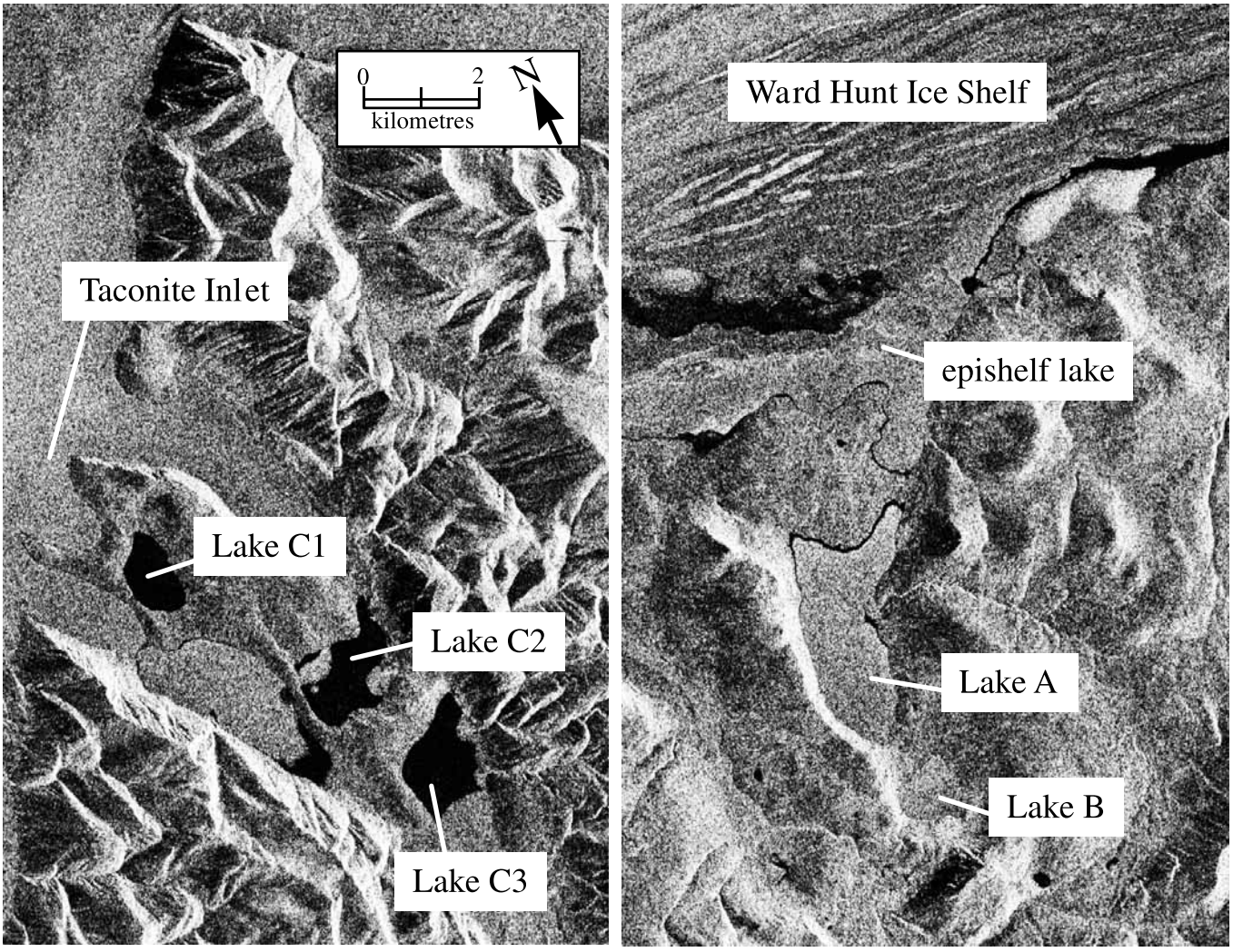

(4) $$E_d(\lambda, z_{snow}) = E_d(\lambda, z_{ice})/(\exp(-K_d(\lambda)_{ice} z_{ice})$$

and $E_d(\lambda, 0^-)$ is equal to $E_d(\lambda, 0^+)$ multiplied by $1 - \alpha(\lambda)_{snow}$.

Water-column irradiance profiles

UVR and PAR under-ice profiles were measured over the deepest part of the lake, with natural snow-cover conditions, using the same PUV500 radiometer as used for transmittance measurements. The PUV500 gave ~15 data points per metre during profiling. Underwater irradiance measurements were corrected for dark current by subtracting the minimum asymptotic value reached at depth. The PUV500 radiometer was lowered through the hole used for $T(\lambda)$ measurements, which was tightly covered with a 1 m^2 opaque board to prevent direct solar radiation from entering the water column through the hole. $K_d(\lambda)$ for the surface freshwater (2–5 m, the 0-m depth being the piezometric water level in the hole) was deter-

mined by linear regression of the natural logarithm of $E_d(\lambda, z)$ versus depth. A vertical profile of the scalar PAR attenuation coefficient (K_0(PAR), m^{-1}) was calculated from E_0(PAR) measured using a PNF300 radiometer (Biospherical Instruments, Inc.). K_0(PAR) was calculated for every 0.5-m interval from the surface to 23 m (the detection limit of the instrument). The beam attenuation coefficient at 660 nm, beam c(660) (m^{-1}), was measured using a Sea Tech transmissometer (Wet Labs, Inc., Philomath, Oreg.) measuring transmission of a collimated light beam over a 10-cm path length.

Chlorophyll *a*

Water samples collected at every metre in the oxic zone (2–12 m) were vacuum-filtered through a 25-mm GF/F-equivalent filter (MFS GF75; Advantec MFS, Inc., Dublin, Calif.). Additional samples were prefiltered through 2-μm Nuclepore filters (Nucleopore Corp., Pleasanton, Calif.) and then onto MFS filters to obtain the picoplanktonic fraction. Filters were stored at –20°C until measurement of chlorophyll *a* (Chl *a*). Chl *a* was extracted with boiling 95% ethanol (Nusch 1980), and the fluorescence of the extract was measured with a model 450 Sequoia–Turner fluorometer (Sequoia–Turner Corp, Mountain View, Calif.). Phaeopigments were corrected for by acidification. For samples collected in the anoxic zone, the absorbance of ethanol extracts of pigments collected on GF/F-equivalent filters was measured using a Hewlett-Packard 8452A diode array spectrophotometer (Hewlett-Packard Corp., Palo Alto, Calif.).

Particulate absorption coefficient

Water samples from selected depths (2, 6.5, 12, 22, and 29 m) were vacuum-filtered in duplicate through 25-mm GF/F filters and stored at –20°C until measurement (10 days after collection) of spectral absorption by particles (a_p). The absorbance of particles concentrated onto the filters was measured every 2 nm over the spectral range 390–800 nm according to Roesler (1998) using a Hewlett-Packard 8452A diode array spectrophotometer equipped with an integrating sphere (Labsphere RSA-HP-84; Hewlett-Packard Corp.). Absorbance values were then converted to a_p using the algorithm of Roesler (1998).

Chromophoric dissolved organic matter (CDOM) absorption coefficient

Measurements of the CDOM absorption coefficient, a_{CDOM} (m^{-1}), were made on each water sample and also for a melted-ice sample taken at ~0.7 m below ice surface and slowly thawed in the dark at 4°C in a plastic Ziploc® bag (S.C. Johnson & Son, Inc., Racine, Wis.). Initial meltwater from this ice sample was discarded to remove any contaminant that may have been transferred during ice drilling and handling. Samples were filtered through 0.22-μm Sartorius cellulose acetate filters (Sartorius, Goettingen, Germany) and stored at 4°C in acid-cleaned, amber glass bottles until analysis (within 4 months). a_{CDOM} was measured every 2 nm over the wavelength range 250–820 nm using a 1-cm, acid-cleaned, quartz cuvette in a Hewlett-Packard 8452A spectrophotometer.

Dissolved organic carbon analysis and CDOM characterization

Dissolved organic carbon (DOC) concentration was determined using the UV Digestion and Infra-red Detection method (Environment Canada, National Laboratory for Environmental Testing). CDOM characterization was made using synchronous fluorescence spectroscopy (Senesi et al. (1991) as modified by J.A.E. Gibson et al., unpublished data). Synchronous fluorescence spectra were recorded with a Shimadzu FR5000 spectrofluorometer (Shimadzu, Kyoto, Japan) used in the synchronous mode with a slit width of 5 nm on both sides and a wavelength difference between the excitation and emission beams of 14 nm, which we have found to be optimal for resolving differences in CDOM between sources. This setting also minimizes the overlap between CDOM peaks and the Raman water peak. Spectra were recorded over the excitation wavelength range 200–600 nm with a corresponding emission range of 214–614 nm. Previous analysis of water samples or isolated fulvic acids from >50 aquatic environments showed that small, autochthonous-like molecules of CDOM (simple aromatic rings without further conjugation) usually show a strong fluorescence peak at 293–308 nm and often show secondary peaks around 360 nm, whereas higher molecular weight molecules with more complex fluorophores (allochthonous-like humic and fulvic materials) fluoresce at longer wavelengths (J.A.E. Gibson et al., unpublished data).

Results

Ice- and snow-cover properties

At the time of sampling, Lake A was covered by 1.97 m (standard deviation (SD) = 0.01 m) of ice. The top 0.12 m was candled ice with long crystals several centimetres in diameter, and the rest was completely fused and clear. No white ice or troughs or ridges at the ice surface were observed. The maximum height of relief on the smooth ice surface was of the order of 10 cm. The top metre of clear ice contained large flattened air bubbles (up to 6 cm long, a few centimetres wide, but only a few millimetres thick). Bubbles were rare and smaller deeper in the ice sheet. Sediment was distributed throughout the top metre of the ice, forming aggregates up to 2 cm in diameter. The piezometric water level was ~13 cm below the ice surface. The snow depths at 1-m intervals along a 20-m transect varied from 39 to 58 cm (average 52 cm, coefficient of variation (CV) = 9%), and the snow surface was flat. At the site of transmittance measurements, the ice was overlaid by 41 cm (CV = 8%, n = 15) of snow. The top ~30 cm was composed of fresh snowflakes and small-grained snow. The deeper layers were composed of loose large crystals typical of deep hoar and indicative of temperature-gradient metamorphism. The average snow density over the full snow profile was 0.21 $g \cdot cm^{-3}$ (as measured gravimetrically using a 6.4-cm-diameter cylinder). The weight of that snow would depress the ice surface by 10 cm. Given the piezometric water level of 13 cm, an average ice density of 0.88 $g \cdot cm^{-3}$ can be deduced.

Irradiance transmittance through the ice and snow cover

The transmittance of PAR and discrete UV wavelengths through the intact ice and snow cover and %T through the ice for a 12-m^2 area cleared of snow are shown in Fig. 3*a*. In presence of the snow cover, 0.45% of incident PAR was transmitted. In the UVR waveband, %T decreased slightly with decreasing wavelength, from 0.46% at 380 nm to 0.31% at 320 nm. Under-ice E_d(305) was below the PUV500 detection limit, preventing %T(305) determination. Removing the snow greatly increased the transmittance; 5.7–6.6% of incident irradiance was transmitted through the ice. The increase was greater at shorter UV wavelengths; this removal of the snow cover resulted in an 18-fold increase in UV at 320 nm and 13-fold in PAR transmittance. Under the conditions of almost eliminated snow cover, the transmittance of 340 nm and 380 nm UV-A was higher than that for

PAR. To calculate the integrated photoinhibiting irradiance prevailing just under the ice, we extended the UVR transmission from the three wavelengths measured by the PUV500 over the full UV spectrum and applied this modeled transmission to the spectral incident irradiance prevailing at noon. This under-ice irradiance was weighted with the biological weighting function for inhibition of photosynthesis from Cullen et al. (1992). Under natural conditions, the weighted under-ice irradiance was only 0.4% of incident. The almost complete removal of snow cover increased photoinhibiting irradiance to 6.3% of incident, a 16-fold increase.

An important part of the difference in %*T* between natural snow conditions and cleared ice was caused by changes in the albedo of the surface. The snow albedo was very high and showed little spectral dependence, varying from 0.94 at 320 nm to 0.97 for PAR (Fig. 3*b*). Once the snow had been removed, the albedo of the candled ice varied from 0.73 at 320 nm to 0.84 for PAR (Fig. 3*b*). Removing the snow cover thus decreased the albedo by 20–22% in the UVR and 13% in the PAR range.

Fig. 3. (*a*) Transmittance through the snow and ice cover (solid bars) of Lake A and through the ice cleared of snow over a 12-m^2 area (open bars). Error bars denote standard deviation (SD) on means from 3 and 4 measurements, respectively. (*b*) Albedo of the snow (solid bars) and candled ice (open bars) surfaces of Lake A. Error bars are SD for 2 and 3 replicated measurements, respectively.

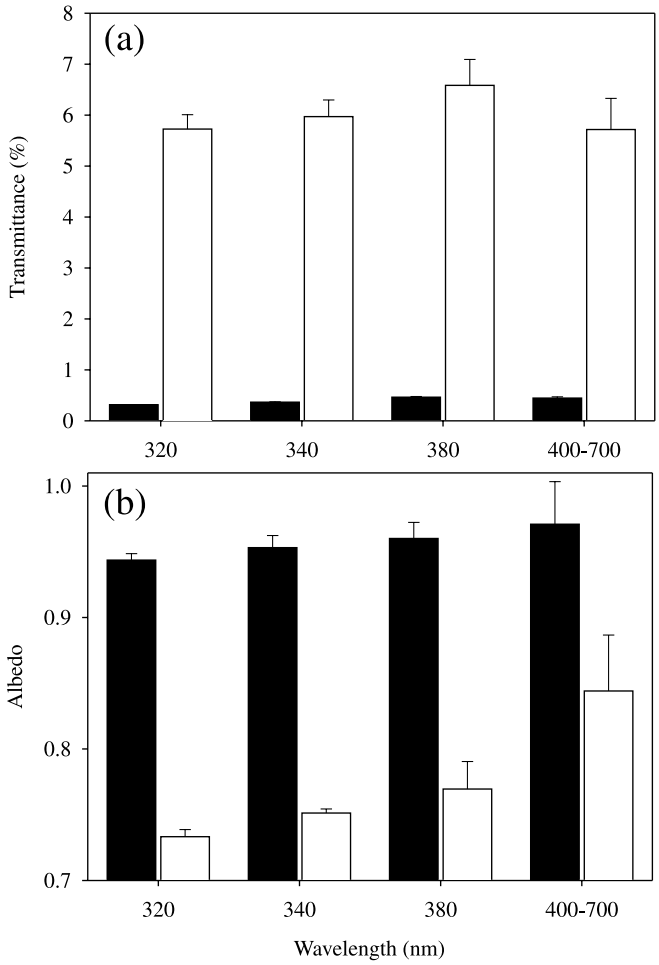

Water-column properties

The vertical profiles of temperature, salinity, and dissolved oxygen showed that the water column was highly stratified (Fig. 4). The top 10-m section of the profile was freshwater with moderately low conductivity (minimum of 0.27 $mS \cdot cm^{-1}$). A chemocline with increasing salinity extended from 10 m to ~28 m; below this depth, the salinity reached ~90% of seawater. The oxic zone extended to 13 m; the percent of oxygen saturation was 120–133% in the top 9 m (probably influenced by oxygen exclusion during ice formation, Wharton et al. 1993) and dropped to 9% at 13 m. Although water temperature was near freezing just under the ice, a thermal maximum of 8.75°C was located at 17.8 m. In the monimolimnion, water temperature gradually decreased with depth to a measured minimum of 4.0°C. The profiles showed no evidence of a mixed isothermal or isohaline layer at any depth.

Spectral irradiance attenuation in the water column

Despite low absolute values, complex patterns of variation of beam *c*(660) were observed down through the water column (Fig. 5). An upper maximum was observed just under the ice, and a second peak began at 29 m and extended to 45 m. A series of irregular, localized peaks were also measured between 12 and 20 m; these peaks are likely associated with Schlieren effects caused by changes in refractive index resulting from the mixing of waters of different salinity during the lowering of the profiler. Below 60 m, beam *c*(660) showed little variability and was slightly higher than the value encountered at 15–20 m. The insert in Fig. 5 compares our beam *c*(660) profile to the one of Ludlam (1996). The large peak measured between 10 and 20 m in late May 1993 was absent in 1999. Also, in 1993, the near-surface maximum was observed very close to the lower ice surface and was only ~1 m thick.

The water column values of $K_d(\lambda)$ were in the low to moderate range for lake waters. The K_d values for UVR in the surface 5 m of the water column were 1.65 (0.28), 1.33 (0.06), and 0.80 (0.10) m^{-1} at 320, 340, and 380 nm, respectively (means of five profiles, SD in parentheses). The equivalent value for PAR was 0.352 (0.089) m^{-1}. In the absence of ice, the 1% depth of 320 nm and 380 nm UVR would be 2.8 m and 5.7 m, respectively, whereas the 1% depth of PAR would be 13.1 m. The large vertical variability in K_0(PAR) matched the beam *c*(660) profile (which is independent of the natural irradiance field), with maximum attenuation just under the ice (K_0(PAR) = 0.347 m^{-1} over the 2- to 5-m depth interval) and lower attenuation between 7 and 14 m (Fig. 6). Only 0.03% of incident E_0(PAR) reached the top of the photosynthetic sulfur bacteria distribution at 16 m (see below) and less than 0.003% at 29 m, the depth of the beam *c*(660) maximum (Fig. 6).

Vertical distribution of optically active particulate and dissolved organic matter

Variations in a_p (Fig. 7) were consistent with the vertical pattern in beam *c*(660). At 22 m, the a_p spectra showed a large absorption peak at 715 nm, typical of bacterio-

Fig. 4. Temperature (thick line), salinity (solid circles), and dissolved oxygen (open circles) profiles in the water column of Lake A. Salinity and dissolved oxygen were measured using an Hydrolab profiler and temperature was measured using a PUV500.

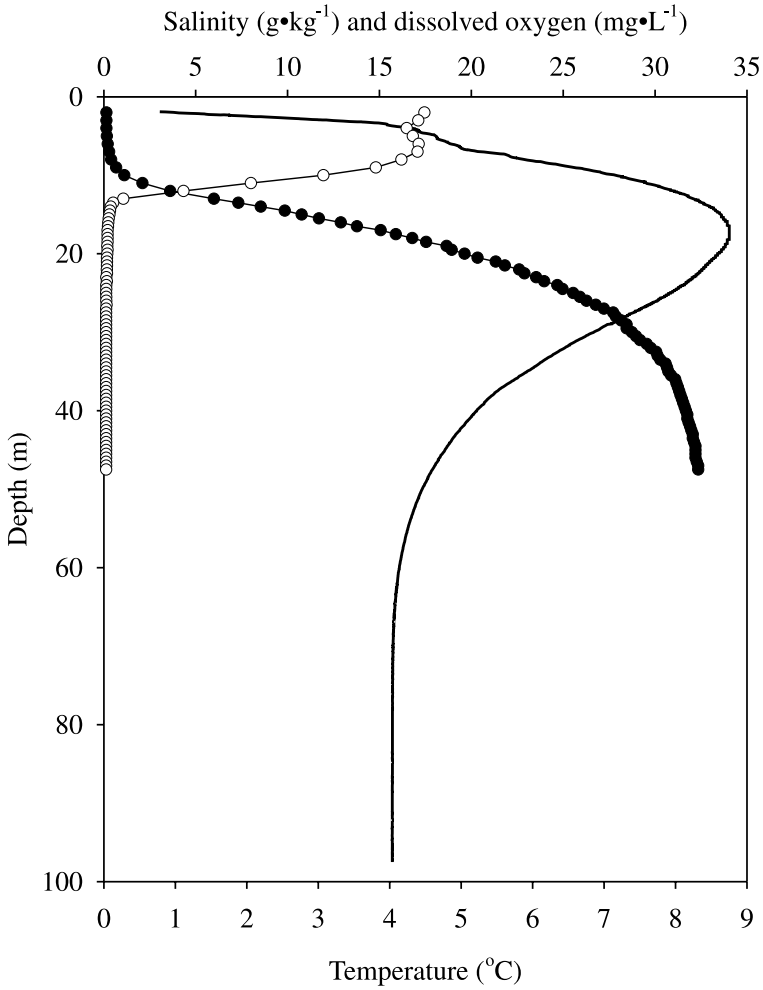

chlorophyll *e* (BChl *e*). The BChl *e* identification was confirmed using methanol extracts and showed the red absorption peak to be centered at 659 nm (Stal et al. 1984). The absorbance of ethanol extracts indicated the absence of BChl *e* above 16 m and maximum concentrations between 20 m and 30 m. The source of this BChl *e* is likely to be green photosynthetic sulfur bacteria of the genus *Chlorobium* (Holt et al. 1993). The absorption maximum found at 29 m (more than two orders of magnitude higher than the a_p measured at other depths; Fig. 7) is probably due to particles of elemental sulfur that accumulate outside these bacterial cells (Holt et al. 1993) superimposed on the BChl *e* absorption peak and possibly also the formation of iron oxides during filtration. The highest a_p in the upper freshwater section of the water column was found just below the ice at a depth of 2 m. The spectral shape of a_p in this oxic zone was typical of phytoplankton, with the red absorption peak at or close to 672 nm, indicative of Chl *a*. The primary Chl *a* absorption maximum was in the blue region of the spectrum, as expected, with an additional broad peak of absorption in the range 530–580 nm, indicative of carotenoids and possibly phycoerythrin (epifluorescence microscopy showed the presence of picocyanobacteria; P. Van Hove et al., unpublished data). The detailed Chl *a* profile in the oxic waters confirmed that Chl *a* concentration was maximal just under the ice (0.43 $\mu g \cdot L^{-1}$) and declined steadily with depth to reach 0.07 $\mu g \cdot L^{-1}$ at 12 m. On average, 62% of the total Chl *a* was contributed by the <2 μm fraction (range 39–97%).

DOC concentrations were low in the upper freshwaters, varying from 0.6 to 1.3 $mg \cdot L^{-1}$ with maximum concentrations just under the ice (Fig. 8). In the monimolimnion, DOC concentrations increased rapidly to reach 3–4 $mg \cdot L^{-1}$; these DOC concentrations are high considering the extreme high latitude position of the lake (cf. Vincent et al. 1998). The vertical distribution of $a_{CDOM}(320)$ followed that of DOC (Fig. 8). However, the DOC-specific $a_{CDOM}(320)$ was low in the freshwater layer (2–3 $m^{-1}(mg \cdot L^{-1})^{-1}$) and increased to 4–5 $m^{-1}(mg \cdot L^{-1})^{-1}$ in the monimolimnion. The much more colored DOC in the monimolimnion suggests a different composition of the DOC pool given that high DOC-specific absorption is usually associated with allochthonous DOC (Morris et al. 1995).

The synchronous fluorescence scans provided further insights into the chemical composition of the DOC and CDOM (Fig. 9). A fluorescence peak occurred at 293–308 nm, indi-

Fig. 5. Beam $c(660)$ profile measured on June 7th, 1999. The insert shows the comparison with Ludlam's (1996) profile measured on May 26, 1993.

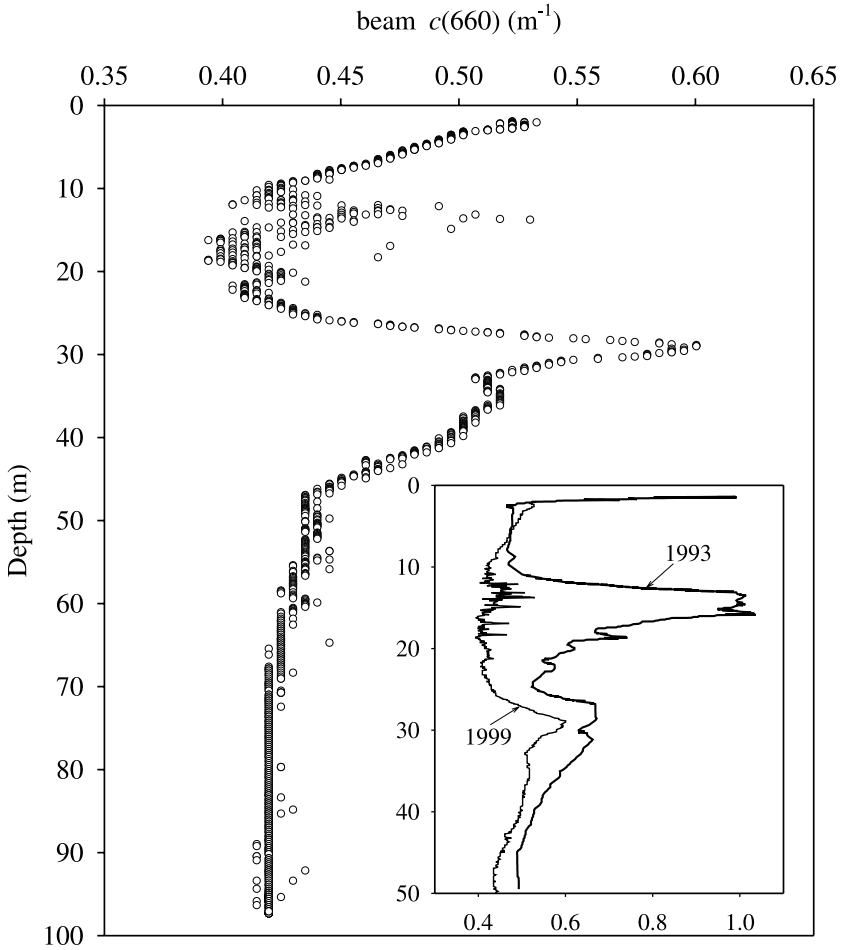

cating that the CDOM in the mixolimnion (Fig. 9*a*) was essentially from microbial origin, in agreement with the low DOC-specific a_{CDOM}. The CDOM in the ice (0.7 m below ice surface) showed a large peak centered at 293 nm that was not found in the scans of samples from the underlying water column. $a_{CDOM}(320)$ in the ice was 1.75 m^{-1}; this value is about half that measured just under the ice and slightly lower than the minimum value measured in the water column (1.85 m^{-1} at 10 m, Fig. 8). From 12 to 20 m, where the brackish waters were suboxic or anoxic, the fluorescence spectra showed a large peak with a maximum at 362 nm and high fluorescence per unit DOC (Fig. 9*b*). Samples from 25 m to the bottom had two additional peaks centered at 392 nm and 491 nm, indicative of large, complex molecules (Fig. 9*c*).

Comparison of snow, ice, and water K_d

Snow K_d(PAR) was 2.1 m^{-1} (Fig. 10*a*), almost an order of magnitude lower than values previously reported (Thomas 1963; Grenfell and Maykut 1977). This striking difference probably results from the low attenuation in the deep hoar layer of the Lake A snow. Snow K_d(UVR) increased with decreasing wavelength to reach 3.3 m^{-1} at 320 nm. Attenuation in the ice was very low compared with that in the snow. Ice K_d(PAR) was 0.32 m^{-1} and K_d increased slightly with decreasing wavelength in the UVR (Fig. 10*a*). The K_d(UVR) for the ice was strikingly lower (up to 53%) than that of the water column, whereas the K_d(PAR) in the ice was 45% higher than in the water column (Fig. 10*b*). Our method of calculation resulted in low effective K_d values for snow and ice. To calculate $K_d(\lambda)_{ice}$, some authors (e.g., Fritsen et al. 1992), rather than using eq. 2, assumed that $E_d(0^-)$ is determined by the specular reflection of $E_d(0^+)$, i.e., $E_d(0^-)$ is approximated to be equal to the incident irradiance reduced by only 2–5%. $K_d(\lambda)_{ice}$ calculated with this $E_d(0^-)$ gives values about two times higher than those calculated using our equations, although the resulting ice $K_d(320)$ is still lower than that of the water column. In the water column, CDOM was responsible for most of the UV and blue light absorption; for example, at 440 nm, CDOM absorption was 0.45 m^{-1} just under the ice, whereas absorption by particles was only 0.04 m^{-1}.

Discussion

Life at the northern limit of lakes

In a previous limnological study of Lake A, Ludlam (1996) suggested that a supersaturated oxygen maximum found just under the ice was related to phytoplankton photosynthesis

Fig. 6. Attenuation coefficient for scalar photosynthetically available radiation (K_0(PAR); open circles) and percent of incident scalar PAR down the water column (thick line). K_0 was determined for 0.5-m depth intervals.

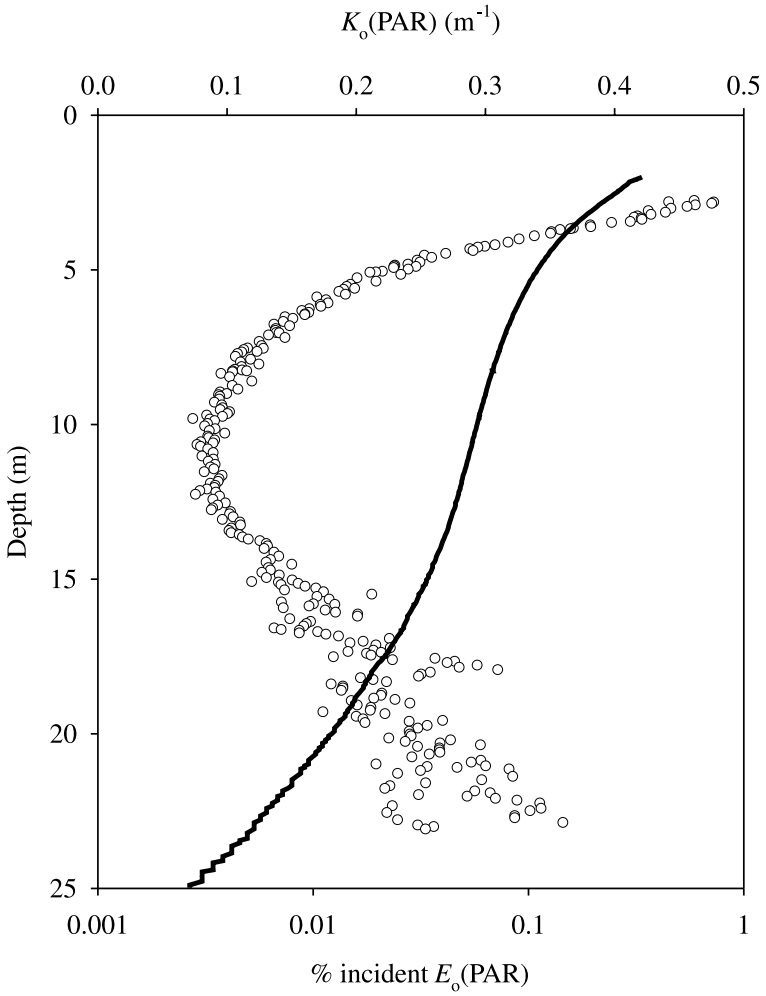

and the deep turbidity maximum was likely due to anoxygenic phototrophic bacteria. The a_p spectra presented here confirm the presence of these hypothesized microbial assemblages and indicate that the deep maximum is dominated by *Chlorobium*. Despite its extreme northern location and thick perennial ice cover, Lake A is inhabited by a complex community of prokaryotic and eukaryotic autotrophs. These autotrophs support an assemblage of small-sized copepods with a mean density of ~400 individuals·m^{-3} in the top 23 m (Van Hove et al. 2001). The presence of macrozooplankton in Lake A represents one important difference relative to the McMurdo LTER perennially ice-covered lakes (Priscu et al. 1999*a*). The low Chl *a* biomass that we measured may be partly due to grazing by copepods, although it may also be related to our sampling early in the growing season. The migration of zooplankton through the water column and their production of fecal pellets is a transport mechanism for organic material in this lake that is absent from the McMurdo lake ecosystems. The bio-optical properties of Lake A's snow and ice cover exert a major influence on all of these planktonic communities by controlling the biological UV exposure and the availability of solar energy for photosynthesis. The large bio-optical and other limnological variations down the water column of Lake A parallel the conditions found in the McMurdo lakes. In these Antarctic systems, as in Lake A, there are major changes in temperature, salinity, and oxygen as a function of depth, with pronounced maxima in bio-optical variables (e.g., Lizotte and Priscu 1992*a*; Vincent et al. 1998). Deep maxima of photosynthetic sulfur bacteria are also found in some Antarctic lakes, for example lakes Fryxell and Hoare (Lizotte and Priscu 1992*a*). In Lake A, peak concentrations of sulfur bacteria pigments were found between 20 m and 30 m, although anoxic conditions start at 14 m. The absence of measurable sulfide in waters above 32 m (J.A.E. Gibson et al., unpublished data) may explain the location of sulfur bacteria well below the oxycline.

Low irradiance attenuation in Lake A ice

The K_d(PAR) for lake ice measured in this study (0.32 m^{-1}) is within the range of ice values for Lake Vanda (0.19–0.67 m^{-1}; Howard-Williams et al. 1998), the clearest of the McMurdo Dry Valleys perennially ice-covered lakes. The dry climate of the Dry Valleys induces the formation of a highly scattering white ice layer at the ice surface as austral summer progresses, decreasing irradiance transmission through the ice (Howard-Williams et al.

Fig. 7. Spectral absorption coefficients of particles at selected depths in the water column of Lake A. Note the different scale for the 29 m spectra (right axis).

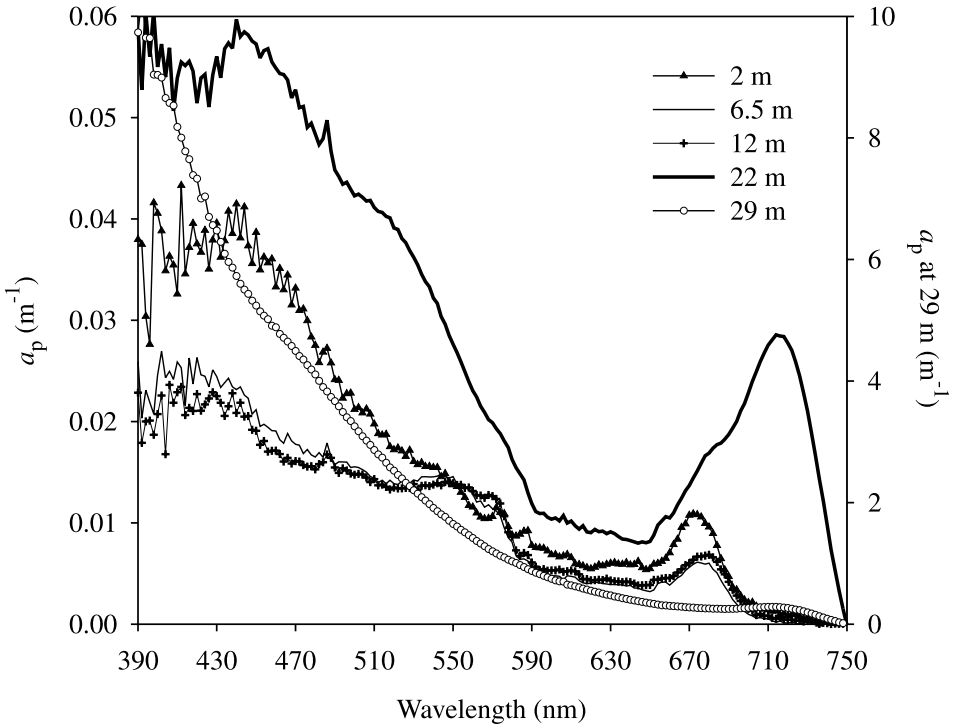

1998; Fritsen and Priscu 1999). Reduction of the transmittance through Antarctic lake ice also results from layers of wind-blown sediment present on top and inside the ice as well as numerous gas bubbles trapped in the ice (Wharton et al. 1993; Adams et al. 1998; Kepner et al. 2000). Sediment was present in the top metre of Lake A ice but as widely spaced aggregates that were unlikely to have a strong influence on the bulk radiative properties of the ice. However, these sediment aggregates are likely to cause melt lenses during summer and to modify bubble structure during freeze-down, thereby indirectly affecting local ice properties (Adams et al. 1998). Gas bubbles were observed although they appeared to be smaller and less numerous than reported for Antarctic lake ice (cf. Adams et al. 1998), presumably because of the lower O_2 and N_2 supersaturation in Lake A. Assuming that the sediment load had a negligible effect on ice buoyancy and given a density ratio of pure ice to water of 0.917 (Adams et al. 1998), the ice-cover density of 0.88 indicates an average air content of the ice cover of only 4%. The 12-cm-thick candled ice of Lake A therefore had a disproportionate impact on irradiance transmission because the remaining ice was so transparent.

The remarkably low K_d(UVR) in the ice relative to the water column of Lake A is likely to be the result of the dilute CDOM content of the ice. We have also measured reduced a_{CDOM} in the 2.3-m-thick ice of Char Lake (Cornwallis Island, 74°42′N); a_{CDOM}(320) in Char Lake ice on June 11, 1999, was 39 and 48% lower at 1 m and 1.5 m, respectively, than in the underlying water column (C. Belzile et al., unpublished data). Priscu et al. (1999*b*) reported the concentration of dissolved organic carbon in bottom accretion ice of Lake Bonney to be 58% of that of the water column, consistent with reduced CDOM in lake ice relative to water. Because of its high absorption in the UVR, CDOM is typically the main optical component controlling UVR attenuation in northern freshwaters (Laurion et al. 1997). The low a_{CDOM} in the ice thus allows Lake A ice to be relatively transparent to UVR despite elevated scattering. PAR attenuation is less affected by CDOM absorption owing to the exponential decrease of a_{CDOM} with increasing wavelength. Accordingly, K_d(PAR) in the ice was higher than in the water column, reflecting the higher scattering in the ice and the much lesser importance for PAR of the large CDOM differences between the ice and water.

Several mechanisms may explain the low a_{CDOM} in the ice. Firstly, freeze-outs of major ions, nutrients, and gases are known to occur during lake-ice formation and are more effective during periods of slow ice growth rate (Wharton et al. 1993; Adams et al. 1998). Ice accretion in Lake A is likely to be slow owing to the insulation provided by the thick ice and the relatively deep snow cover. Photochemical processes may contribute to a decrease of a_{CDOM} in the ice and may contribute to the fluorescence peaks indicative of small, simple molecules. Despite the short Arctic summer, the perennial nature of Lake A ice would allow relatively long exposure to UVR and the possibility of gradual photodegradation of DOC within the ice sheet. Finally, the sediment aggregates found in the top metre of the ice may be the site of microbial activity when liquid water is present, equivalent to the microbial consortium recently discovered in Antarctic lake ice (Priscu et al. 1998). Microbial degradation processes could accelerate the breakdown of CDOM. This biological activity may also result in autochthonous DOC production (Priscu et al. 1998), which could further explain spectral fluorescence peaks of small, simple molecules. In lakes of the Queen Maud Land (Antarctica), Kaup (1988) found situations where ice K_d(PAR) did not exceed that of

Fig. 8. Dissolved organic carbon concentrations (DOC; solid circles) and chromophoric dissolved organic matter absorption coefficients at 320 nm ($a_{CDOM}(320)$; open triangles) down the water column of Lake A.

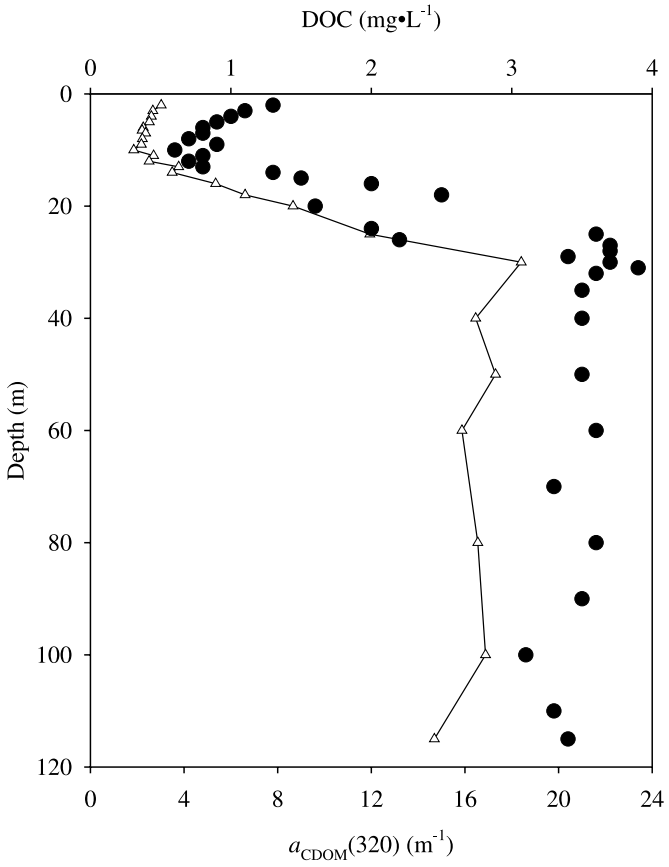

the underlying water column. He noted that the ice crystals of the perennially ice-covered Lake Untersee can have diameters of 20 cm and more and can extend through the 3-m-thick ice. He postulated that these vertically oriented crystals act as light conductors, resulting in the very low K_d(PAR) for this type of ice. This situation may also apply to Lake A ice and the combination of low scattering and low absorption inside the ice crystals would allow relatively high UVR transmission through the ice.

Although the ice itself is relatively transparent to solar irradiance, the high albedo and K_d of the snow considerably reduced the irradiance reaching the water column. In early June, although solar irradiance was near its maximum, phytoplankton cells directly under the ice received at best 5 µmol photons·m^{-2}·s^{-1} of PAR. This is likely to cause severe light limitation. For example, even the highly shade-adapted phytoplankton in the McMurdo ice-covered lakes have light saturation values for photosynthesis of 10–30 µmol photons·m^{-2}·s^{-1} (Lizotte and Priscu 1992*b*).

Importance of CDOM in the water column

The attenuation coefficient of scalar PAR measured by Ludlam (1996) in the surface waters of Lake A was 0.304 m^{-1}, in good agreement with the value of 0.347 m^{-1} reported here. Water column K_d(PAR) and K_d(UVR) were low, although they were higher than those found, using the same radiometer, in perennially ice-covered lakes Vanda, Bonney, and Hoare in the McMurdo region (Vincent et al. 1998). This is consistent with the lower DOC concentrations recorded in these Antarctic lakes. UV attenuation in Lake A was similar to that measured in Lake Fryxell by Vincent et al. (1998), although DOC concentration is at least two times higher in the latter lake (McKnight et al. 1991; Vincent et al. 1998). It is likely that the DOC in these lakes is less colored than in Lake A, given their extremely barren catchments and the dominance by autochthonous processes in controlling their carbon dynamics. Approximately 5–10% of the ground around Lake A is covered with vegetation, mostly cushion plants (*Saxifraga oppositifolia*) but also some herbs and shrubs (including *Salix arctica* and *Dryas integrifolia*) (E. Lévesque, Université du Québec à Trois-Rivières, Trois-Rivières, Québec, unpublished data). These plants likely contribute to the allochthonous DOC input to the lake. As in Lake A, DOC concentrations increase with depth in most Antarctic perennially ice-covered lakes (e.g., from 1.3 to 3.9 mg·L^{-1} in Lake Hoare and from 3.3 to 30 mg·L^{-1} in Lake Fryxell; McKnight et al. 1991). McKnight et al. (1991) showed that the fulvic acid (FA) fraction of the DOC in lakes Hoare and Fryxell had similar elemental compositions, carbon distributions, and amino acid contents, indicating that the chemistry of these microbially derived FA is not strongly influenced by the chemical environment in the water column. However, the FA fraction represented only 16–20% of total DOC in these lakes. The very different fluorescence properties of CDOM observed through the water column of Lake A suggest that major differences in the composition of the DOM pool exist as a function of depth. The processes responsible for the presence in the suboxic and anoxic layers of CDOM with fluorescence characteristics typical of large and complex molecules remains to be elucidated. This fluorescent material may be remnant from the original DOC-containing ocean water that originally filled the basin or, more likely, may be the result of chemical (e.g., through sulfurisation by reaction with sulfide) or biological transformation of the simple material originating from the surface waters. These presumed modifications of the DOC pool are conspicuous in Lake A because of the highly stratified nature of the water column, but they are also likely to occur in other aquatic ecosystems. CDOM can be an important precursor of carbon substrates for heterotrophic growth and may help support mixotrophic phytoplankton during the long period of winter darkness (Priscu et al. 1999*a*).

In Lake A, UVR attenuation in the water column and ice would provide sufficient protection against UV damage to the photosynthetic sulfur bacteria growing below 13 m. The phytoplankton growing immediately under the ice are exposed to higher UVR fluxes, up to 6.3% of incident photoinhibiting solar irradiance under snow-free conditions (based on our snow-clearing experiment). Moreover, the ice surface artificially cleared of snow probably had a higher albedo because of the small residual amounts of snow trapped in the irregular ice surface and the influence of the snow at the edge of the cleared area. The air-filled candled ice was also likely more scattering than under melting conditions when liquid water ponding on the ice surface would substantially reduce the albedo. The irradiance transmission in natural

Fig. 9. Dissolved organic carbon specific synchronous fluorescence spectroscopy scans of chromophoric dissolved organic matter from the lake ice and selected depths in the water column.

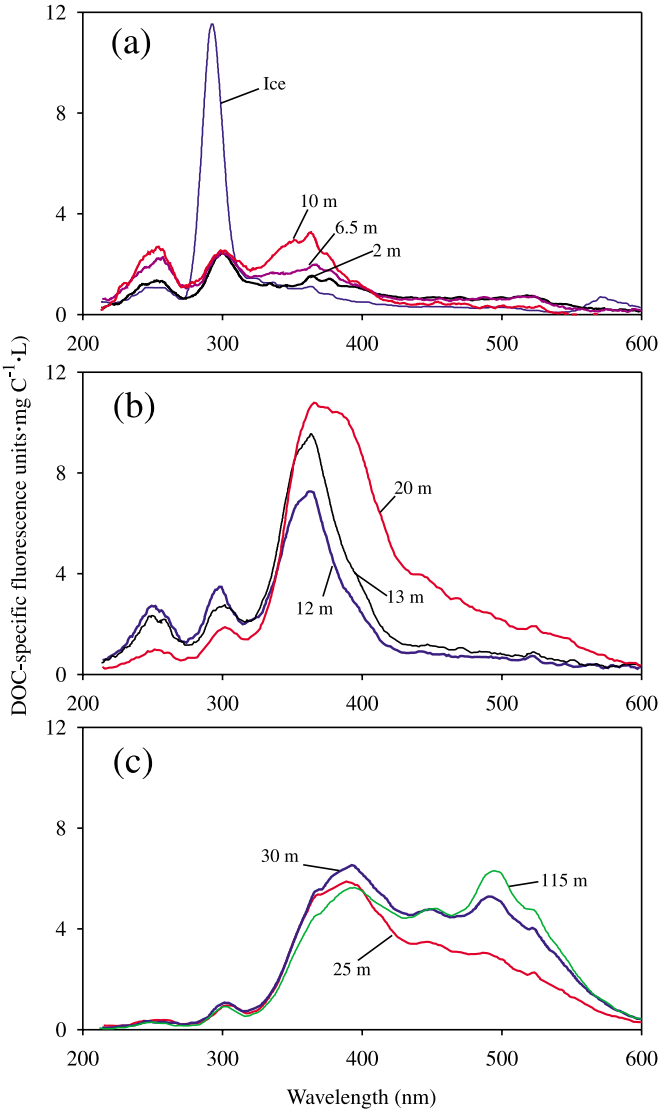

snow-free conditions is therefore likely to be higher than that measured here, unless significant "ice whitening" similar to that observed in Antarctic perennially ice-covered lakes (Fritsen and Priscu 1999) is occurring.

Climate change

Given the relative transparency of the ice cover, the opaque nature of the snow, and the strong seasonal variations in incident irradiance (complete darkness from mid-October until the end of February), most of the annual input of solar energy to the lake must be restricted to a brief period of the year. Simple model calculations based on K_d and assuming no change in surface albedo show that a 20% variation in snow depth would correspond to a similar percent change in the amount of PAR entering the lake (from $\%T$ = 0.50% with z_{snow} = 41 cm to 0.41% and 0.60% with 49 cm and 22 cm of snow, respectively). However, the removal of snow over a 12-m^2 area increased $\%T$(PAR) 13 times and would

Fig. 10. (*a*) Snow (solid bars), ice (open bars), and water-column (hatched bars) attenuation coefficients for downwelling irradiance, $K_d(\lambda)$. Error bars for water-column $K_d(\lambda)$ are standard deviations for the means of five different profiles. (*b*) Percent change of $K_d(\lambda)$ in the ice relative to that in the water.

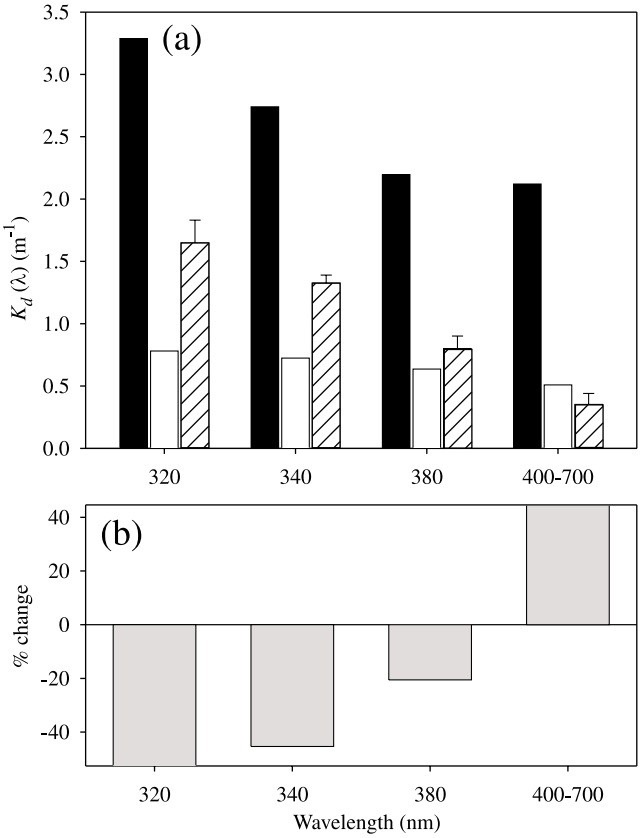

increase photoinhibiting UVR 16 times. Changes in the timing of the disappearance of snow cover would have a major impact on the annual radiation budget of the lake, with implications for stratification, mixing, and biological processes.

There is no statistical trend in the temperature or precipitation at Alert for the period 1951–1999 (C. Belzile et al., unpublished data). However, for the last 32 years of this record, there has been a significant warming trend in mean annual temperature (0.04°C per annum) and a highly significant decline in the number of freezing degree-days per annum (loss of 15 freezing degree-days per annum; Vincent et al. 2001). These most recent trends are likely to be related, at least in part, to the Arctic Oscillation, although they may also be amplified by anthropogenic forcing (Rigor et al. 2000).

There is considerable interannual variability in the Alert climate record. For example, snow depth at Alert at the end of the cold season ranged from 9 to 79 cm for the period 1949 to 1988 (Curtis et al. 1998), and a difference of 27 days was shown between the earliest (June 4th) and latest (July 1st) date of the onset of snowmelt (Table 1). Such variations in the thickness and duration of snow cover over the perennial ice of Lake A would translate into major interannual differences in the annual solar energy input to the lake and are likely to cause pronounced year-to-year differences in biological productivity. Despite this variability,

however, the ice has remained on the lake on all years of direct or remote observation.

Changes greater than the interannual variability will accompany future warming trends in the region, as predicted by global models (Weller 1998). Relatively minor increases in air temperature beyond the 1998 maximum could cause the complete loss of ice cover of Lake A. Our optical results reported here show that such a change would completely alter the limnological characteristics of this High Arctic ecosystem.

Acknowledgments

This research was funded by the Natural Sciences and Engineering Research Council of Canada, the Fonds pour la Formation de Chercheurs et l'Aide à la Recherche of Quebec, the Centre d'études nordiques, and Indian and Northern Affairs Canada. We thank Polar Continental Shelf Project for logistic support in the Arctic (this is PCSP publication number 03101) and Robert Gauthier and the staff of the Canadian Center for Remote Sensing for their help in the acquisition of RADARSAT imagery. We also thank Peter T. Doran and an anonymous reviewer for insightful comments.

References

Adams, E.E., Priscu, J.C., Fritsen, C.H., Smith, S.R., and Brackman, S.L. 1998. Permanent ice covers of the McMurdo Dry Valleys lakes, Antarctica: bubble formation and metamorphism. Antarct. Res. Ser. **72**: 281–295.

Bolsenga, S.J., Evans, M., Vanderploeg, H.A., and Norton, D.G. 1996. PAR transmittance through thick, clear freshwater ice. Hydrobiologia, **330**: 227–230.

Cullen, J.J., Neale, P.J., and Lesser, M.P. 1992. Biological weighting function for the inhibition of phytoplankton photosynthesis by ultraviolet radiation. Science (Washington, D.C.), **258**: 646–650.

Curtis, J., Wendler, G., Stone, R., and Dutton, E. 1998. Precipitation decrease in the western Arctic, with special emphasis on Barrow and Barter Island, Alaska. Int. J. Climatol. **18**: 1687–1707.

Doran, P.T., Wharton, R.A., Jr., and Lyons, W.B. 1994. Paleolimnology of the McMurdo Dry Valleys, Antarctica. J. Paleolimnol. **10**: 85–114.

Doran, P.T., McKay, C.P., Adams, W.P., English, M.C., Wharton, R.A., Jr., and Meyer, M.A. 1996. Climate forcing and thermal feedback of residual lake-ice covers in the High Arctic. Limnol. Oceanogr. **41**: 839–848.

Ellis-Evans, J.C., Laybourn-Parry, J., Bayliss, P.R., and Perriss, S.J. 1998. Physical, chemical and microbial community characteristics of lakes of the Larsemann Hills, Continental Antarctica. Arch. Hydrobiol. **141**: 209–230.

Fofonoff, N.P., and Millard, R.C. 1983. Algorithms for the calculations of fundamental properties of seawater. UNESCO Technical Papers in Marine Science 44. UNESCO, Paris, France.

Fritsen, C.H., and Priscu, J.C. 1999. Seasonal change in the optical properties of the permanent ice cover on Lake Bonney, Antarctica: consequences for lake productivity and phytoplankton dynamics. Limnol. Oceanogr. **44**: 447–454.

Fritsen, C.H., Iturriaga, R., and Sullivan, C.W. 1992. Influence of particulate matter on spectral irradiance fields and energy transfer in the eastern Arctic Ocean. Ocean Optics XI SPIE, **1750**: 527–541.

Grenfell, T.C. 1991. A radiative transfer model for sea ice with vertical structure variations. J. Geophys. Res. **96**: 16 991–17 001.

Grenfell, T.C., and Maykut, G.A. 1977. The optical properties of ice and snow in the Arctic Basin. J. Glaciol. **18**: 445–463.

Hanssenbauer, I., and Forland, E.J. 1998. Long-term trends in precipitation and temperature in the Norwegian Arctic: can they be explained by changes in atmospheric circulation patterns. Clim. Res. **10**: 143–153.

Hattersley-Smith, G., Keys, J.E., Serson, H., and Mielke, J.E. 1970. Density stratified lakes in Northern Ellesmere Island. Nature (London), **225**: 55–56.

Holt, J.G., Krieg, N.R., Sneath, P.H.A., Staley, J.T., and Williams, S.T. 1993. Bergey's manual of determinative bacteriology. 9th ed. Williams & Wilkins, Baltimore, Md.

Howard-Williams, C., Schwarz, A.-M., Hawes, I., and Priscu, J.C. 1998. Optical properties of McMurdo Dry Valleys lakes, Antarctica. Antarct. Res. Ser. **72**: 189–203.

Jeffries, M.O., Krouse, H.R., Shakur, M.A., and Harris, S.A. 1984. Isotope geochemistry of stratified Lake "A," Ellesmere Island, N.W.T., Canada. Can. J. Earth Sci. **21**: 1008–1017.

Johannessen, O.M., Shalina, E.V., and Miles, M.W. 1999. Satellite evidence for an Arctic sea ice cover in transformation. Science (Washington, D.C.), **286**: 1937–1939.

Kaup, E. 1988. Solar radiation in the water bodies of Queen Maud Land. *In* Limnological studies in Queen Maud Land (East Antarctica). *Edited by* J. Martin. Academy of Sciences of the Estonian SSR, Tallinn, Estonia, USSR. pp. 15–27.

Kepner, R.L., Wharton, R.A., Jr., Collier, R.D., Cockell, C.S., and Jeffrey, W.H. 2000. UV radiation and potential biological effects beneath the perennial ice cover of an antarctic lake. Hydrobiologia, **427**: 155–165.

Laurion, I., Vincent, W.F., and Lean, D.R.S. 1997. Underwater ultraviolet radiation: development of spectral models for northern high latitude lakes. Photochem. Photobiol. **65**: 107–114.

Lizotte, M.P., and Priscu, J.C. 1992*a*. Spectral irradiance and bio-optical properties in perennially ice-covered lakes of the Dry Valleys (McMurdo Sound, Antarctica). Antarct. Res. Ser. **57**: 1–14.

Lizotte, M.P., and Priscu, J.C. 1992*b*. Photosynthesis–irradiance relationships in phytoplankton from the physically stable water column of a perennially ice-covered lake (Lake Bonney, Antarctica). J. Phycol. **28**: 179–185.

Ludlam, S.D. 1996. The comparative limnology of high arctic, coastal, meromictic lakes. J. Paleolimnol. **16**: 111–131.

Madronich, S., McKenzie, R.L., Björn, L.O., and Caldwell, M.M. 1998. Changes in biologically active ultraviolet radiation reaching the Earth's surface. J. Photochem. Photobiol. B, Biol. **46**: 5–19.

McKnight, D.M., Aiken, G.R., and Smith, R.L. 1991. Aquatic fulvic acids in microbial based ecosystems: results from two desert lakes in Antarctica. Limnol. Oceanogr. **36**: 998–1006.

Morris, D.P., Zagarese, H., Williamson, C.E., Balseiro, E.G., Hargreaves, B.R., Modenutti, B., Moeller, R., and Queimalinos, C. 1995. The attenuation of solar UV radiation in lakes and the role of dissolved organic carbon. Limnol. Oceanogr. **40**: 1381–1391.

Nusch, E.A. 1980. Comparison of different methods for chlorophyll and phaeopigment determination. Arch. Hydrobiol. Beih. **14**: 14–36.

Perovich, D.K., Roesler, C.S., and Pegau, W.S. 1998. Variability in Arctic sea ice optical properties. J. Geophys. Res. **103**: 1193–1208.

Priscu, J.C. 1998. Ecosystem processes in a polar desert: the McMurdo Dry Valleys, Antarctica. Antarct. Res. Ser. Vol. 72. American Geophysical Union, Washington, D.C.

Priscu, J.C., Fritsen, C.H., Adams, E.E., Giovannoni, S.J., Paerl, H.W., McKay, C.P., Doran, P.T., Gordon, D.A., Lanoil, B.D., and Pinckney, J.L. 1998. Perennial Antarctic lake ice: an oasis for life in a polar desert. Science (Washington, D.C.), **280**: 2095–2098.

Priscu, J.C., Wolf, C.F., Takacs, C.D., Fritsen, C.H., Laybourn-Parry, J., Roberts, E.C., Sattler, B., and Lyons, W.B. 1999*a*. Carbon transformation in a perennially ice-covered Antarctic lake. BioScience, **49**: 997–1008.

Priscu, J.C., Adams, E.E., Lyons, W.B., Voytek, M.A., Mogk, D.W., Brown, R.L, McKay, C.P., Takacs, C.D., Welch, K.A., Wolf, C.F., Kirshtein, J.D., and Avci, R. 1999*b*. Geomicrobiology of subglacial ice above Lake Vostok, Antarctica. Science (Washington, D.C.), **286**: 2141–2144.

Rigor, I.G., Colony, R.L., and Martin, S. 2000. Variations in surface air temperature observations in the Arctic, 1979–97. J. Clim. **13**: 896–914.

Roesler, C.S. 1998. Theoretical and experimental approaches to improve the accuracy of particulate absorption coefficients derived from the quantitative filter technique. Limnol. Oceanogr. **43**: 1649–1660.

Rothrock, D.A., Yu, Y., and Maykut, G.A. 1999. Thinning of the Arctic sea-ice cover. Geophys. Res. Lett. **26**: 3469–3472.

Senesi, N., Miano, T.M., Provenzano, M.R., and Brunetti, G. 1991. Characterization, differentiation, and classification of humic substances by fluorescence spectroscopy. Soil Sci. **152**: 259–271.

Shindell, D.T., Rind, D., and Lonergan, P. 1998. Increased polar stratospheric ozone losses and delayed eventual recovery owing to increasing greenhouse-gas concentrations. Nature (London), **392**: 589–592.

Stal, L.J., van Gemerden, H., and Krumbein, W.E. 1984. The simultaneous assay of chlorophyll and bacteriochlorophyll in natural microbial communities. J. Microbiol. Methods, **2**: 295–306.

Thomas, C.W. 1963. On the transfer of visible radiation through sea ice and snow. J. Glaciol. **4**: 481–484.

Van Hove, P., Swadling, K.M., Gibson, J.A.E., Vincent, W.F., and Belzile, C. 2001. Farthest north lake and fjord populations of calanoid copepods *Limnocalanus macrurus* and *Drepanopus bungei* in the Canadian High Arctic. Polar Biol. **24**: 303–307.

Vincent, W.F., Rae, R., Laurion, I., Howard-Williams, C., and Priscu, J.C. 1998. Transparency of Antarctic ice-covered lakes to solar UV radiation. Limnol. Oceanogr. **43**: 618–624.

Vincent, W.F., Gibson, J.A.E., and Jeffries, M.O. 2001. Ice-shelf collapse, climate change and habitat loss in the Canadian High Arctic. Polar Rec. **37**: 133–142.

Welch, H.E., and Kalff, J. 1974. Benthic photosynthesis and respiration in Char Lake. J. Fish. Res. Board Can. **31**: 609–620.

Weller, G. 1998. Regional impacts of climate change in the Arctic and Antarctic. Ann. Glaciol. **27**: 543–552.

Wharton, R.A., Jr., McKay, C.P., Clow, G.D., and Andersen, D.T. 1993. Perennial ice covers and their influence on Antarctic lake ecosystems. Antarct. Res. Ser. **59**: 53–70.